RSC Advances

ROYAL SOCIETY OF CHEMISTRY

www.rsc.org/advances

One-step electrochemical preparation and characterization of nanostructured hydrohausmannite as electrode material for supercapacitors

M. Aghazadeh, [a,†] M. Ghannadi Maragheh, [a] M. R. Ganjali [b,c] and P. Norouzi [b]

[a,†] *Nuclear Science and Technology Research Institute (NSTRI), P.O. Box 14395-834, Tehran, Iran. E-mail address: mustafa.aghazadeh@gmail.com*

[b] *Center of Excellence in Electrochemistry, Faculty of Chemistry, University of Tehran, Tehran, Iran*

[c] *Biosensor Research Center, Endocrinology and Metabolism Molecular-Cellular Sciences Institute, Tehran University of Medical Sciences, Tehran, Iran*

Abstract

A novel, simple one-pot electrochemical procedure is proposed for the preparation hydrohausmannite. The deposition experiments were performed in manganese chloride bath under a galvanostatic mode, applying a current density of 2 mA cm^{-2} (I_a= 2 mA cm^{-2}). The structural characterizations with XRD and FTIR revealed the prepared sample to be composed of mixed Mn_3O_4 and MnOOH phases which is known as hydrohausmannite. Morphological evaluations by SEM and TEM further proved that the prepared sample had a nanoscale particle/plate morphology and the electrochemical measurements through cyclic voltammetry (CV) and charge-discharge techniques revealed that the prepared hydrohausmannite had an excellent capacitive behavior, with the specific capacitance values of 232, 209, 184, 133, 99 and 89 F g^{-1} were calculated at the scan rates of 5, 10, 20, 50, 100 and 125 mV s^{-1}, respectively. An excellent long-term cycling stability of 92% was also observed after 1000 charge–discharge cycles.

1 Introduction

Supercapacitors, also called electrochemical capacitors, are classified into two types of electrochemical double layer capacitors or electric double layer capacitors (EDLCs) and pseudocapacitors. The former type stores energy through charge accumulation at the electrode/electrolyte interface in the form of an electrical double layer while pseudocapacitors reserve energy based on redox reactions, i.e., oxidation-reduction reactions on a surface of an electrode material. Research in the area of EDLCs focuses on porous carbon materials including graphene, activated carbon, and carbon nanotubes (CNTs) that offer high surface areas and readily accessible mesoporous.[1] Investigation in the field of pseudocapacitors, on the other hand, centres around transition metal oxides, which have received great attention due to their high capacitance values of 200-1300 F/g as compared to that the values of 50-150 F/g in the case of material used in EDLCs.[2] Manganese oxides have been considered as excellent supercapacitor electrode materials due to their ideal capacitive behavior, environmental compatibility and low cost.[3–5] Among these compounds Mn_3O_4 has been the subject of relatively less research compared to MnO_2. Hydrohausmannite, which was introduced by Feitknecht,[6] is a mixture of *β*-MnOOH and *γ*-Mn_3O_4. Hydrohausmannite structure is chemically similar to hausmannite ($MnMn_2O_4$) with some variation in the ratio of Mn^{2+} to Mn^{3+}. This variation is compensated by substitution of O with OH.[6] The typical morphology of hydrohausmannite has been also reported to include hexagonal plates and particles.[7] Additionally, hexagonal plates and particles have generally been recognized as *β*-MnOOH and *γ*-Mn_3O_4 respectively.[7] Ya *et al.* prepared hydrohausmannite through a hydrothermal method and adjusted the experimental parameters to obtain a hexagonal plate morphology for the prepared hydrohausmannite, and found that *β*-MnOOH and *γ*-Mn_3O_4 can exist in both possible morphologies of hydrohausmannite i.e. particle and plate.[8]

Until now, hydrohausmannite has been rarely studied and only two reports are available on this material in literature, [8,9] both of which deal with the hydrothermal preparation of hydrohausmannite nanoplates. So, the preparation of hydrohausmannite nanostructures through any chemical and electrochemical synthetic routes can be regarded as an interesting, yet unexplored area of research. It was reported that electrochemical route is a powerful technique in the production of nanostructured manganese oxides including α-, β-,γ- and λ-MnO_2, Mn_3O_4 and Mn_2O_3.[10–21] The most significant advantage of this clean and

inexpensive family of techniques is its power to control the structural and morphological properties of the deposited products through the manipulation of parameters such as current density, potential, concentration, pH, temperature, nature of the surfactant or substrate. Both anodic and cathodic electrodeposition techniques can be used for the preparation of manganese oxides. The former suffers disadvantages like anodic oxidation, and dissolution of the current collector and substrate, which have been overcome by the latter technique, i.e. the cathodic electrodeposition. So, cathodic electrodeposition, as an interesting method, can be used for preparation of hydrohausmannite.

Herein, we wish to report the preparation of nanostructured hydrohausmannite through a novel, simple and facile one-pot cathodic electrodeposition method. The results of our experiments showed that the particle/plate nanostructures of hydrohausmannite can be simply prepared via galvanostatic cathodic deposition from aqueous manganese chloride solutions. To the best our knowledge, the electrochemical method has not been applied for the preparation of hydrohausmannite. And there is no report regarding to the cathodic electrodeposition of nanostructured hydrohausmannite. Notably, only hydrothermal method has been used for preparation of this material.[8,9] In these reports, hydrothermal as an chemical rout has been developed for the synthesis of nanoplates of hydrohausmannite. This method needs a mixed solution, heating at 200 ^{o}C for 72h and then cooling, repeatedly washing with deionized water and ethanol, then drying at 60 ^{o}C for 10h. While our used electrochemical method i.e. cathodic electrodeposition has one-pot, simple and easy route and no need for heat treatment. In fact, the nanostructured hydrohausmannite is simply prepared by applying current density of 2 mA cm^{-2} into an additive-free solution of 0.005 $MnCl_2$ for 30 min at RT.

It should be noted that the supercapacitive performance of hydrohausmannite has been rarely reported and only one work has been performed in this regard. Dan et al. [9] investigated the electrochemical performance of the hydrohausmannite nanoplates prepared by hydrothermal method. Electrochemical tests via cyclic voltammetry and charge-discharge revealed that the nanoplates are capable to deliver a specific capacitance as high as 222.4 F g^{-1} at the applied current density of 0.1 A g^{-1}, and also good rate capability (66.7 F g^{-1} at 6 A g^{-1}) was observed. Based on the obtained results, they concluded that hydrohausmannite may have great potential applications in supercapacitor electrode material. However, to be able to judge the results of this work and the properties of the product, the electrochemical

properties of the prepared nanostructured hydrohausmannite were investigated by cyclic voltammetry and galvanostatic charge–discharge measurements. The electrodeposited nanoplates possess an specific capacitance as high as 239 F g^{-1} calculated from discharge curve with current density 1 mA cm^{-2}, and the capacity retentions of 92%, 81%, 74%, 62% and 47% at the applied current densities of 2, 5, 7, 10 and 15 mA cm^{-2}, respectively, as compared to the low applied current density of 1 mA cm^{-2}. These values implied that the prepared sample exhibits good cycling and rate capability as active electrode material for supercapacitor. Furthermore, comparing the obtained results with the electrochemical performances of other MnO_x or MnOOH capacitor materials confirmed that the hydrohausmannite nanoplates have good electrochemical properties which make them as a potential candidate for use in supercapacitors.

2 Experimental section

2.1 Chemicals

$MnCl_2$.$6H_2O$ (Merck), polytetrafluoroethylene (PTFE, Merck), carbon black and Na_2SO_4 (Merck) were used as received. All solutions were prepared using water purified by a UHQ Elga System. An aqueous solution of 5 mM $MnCl_2$.$6H_2O$ was prepared for electrodeposition.

2.2 Preparation procedure

Hydrohausmannite was prepared by a novel one step cathodic electrodeposition method as below. The deposition experiments were performed in a two electrode electrochemical cell including a steel (316L) cathode and graphite anode. An aqueous 0.005M $MnCl_2$.$6H_2O$ solution was used as the electrolyte. A direct current (DC) regime (I=2 mA cm^{-2}) was applied in the deposition process. The deposition time and bath temperature were 30 min and 25 ^oC, respectively. Prior to each deposition, the steel substrate was given a galvanostatically electropolishing. The deposition experiments were performed using an electrochemical workstation system (Potentiostat/Galvanostat, Model: NCF-PGS 2012, Iran). After the deposition, the steel substrates were repeatedly rinsed with water and then dried at RT for 5h. Finally the deposits were scraped from the substrates and evaluated by further analyses.

2.3 Characterization

The phase composition and structure of the prepared samples were investigated by powder X-ray diffraction (XRD) using a Phillips PW-1800 diffractometer with a Cu Kα radiation source in 2θ values ranging from 5 to 70°C at a scanning rate of 5 degree/min. The FTIR spectra of the samples were obtained using a Bruker Vector 22 Fourier transformed infrared spectroscope in the range of 400–4000 cm^{-1}. The samples were prepared in a KBr wafer and the analyses were performed at ambient temperature,. Each FTIR spectrum was acquired after 20 scans at a resolution of 4 cm^{-1} from 400 to 4000 cm^{-1}.The morphologies of the prepared hydrohausmannite powder were studied using a scanning electron microscope (SEM, LEO 1455 VP, Oxford, UK, operating voltage 30 kV). Transmission electron microscopy (TEM) images were also acquired using a Phillips EM 208 transmission electron microscope with an accelerating voltage of 100 kV.

2.4 Electrochemical measurements

The working electrodes were fabricated by mixing the prepared hydrohausmannite powder (80 wt.%), carbon black (15 wt.%) and polytetrafluorene ethylene (PTFE, 5 wt.%). Next a small amount of ethanol was added to the mixture to produce a homogeneous paste and the mixture was pressed onto steel grid (surface area=1 cm^2) current collectors to form the working electrodes. The electrochemical performances of the prepared working electrodes were performed in a conventional three electrode cell filled with a 1 M Na_2SO_4 solution as the electrolyte. A platinum foil and an Ag/AgCl (saturated with 1 M KCl) electrode were used as the counter and reference electrodes, respectively. For the electrochemical measurements, a homemade potentiostat according to our previous works[22,23] was used. The cyclic voltammetric (CV) studies were conducted in a potential range of between -0.2 and 0.8 V versus Ag/AgCl at various scan rates of 5, 10, 20,50, 100 and 125 mV s^{-1}. The constant current charge–discharge tests were carried out at different current densities of 1, 2, 5, 10 and 15 mA cm^{-2} within a potential range of -0.2 to 0.8 V versus Ag/AgCl reference electrode.

3 Results and discussion

3.1 Structural characterization

Fig. 1 shows the XRD pattern of the sample prepared in the electrodeposition process. All peaks of the pattern can be well indexed to feitknechtite (β-MnOOH, JCPDS No. 18-0804) and hausmannite (γ-Mn_3O_4, JCPDS No. 80-0382)with *a*=0.576 nm and *c*=0.947 nm, as donated by symbols in the pattern. This mixed phases was previously recognized as pure single phase i.e. hydrohausmannite.[6-8] No peak, related to any impurities, was observed in the XRD pattern, which confirmed that a pure hydrohausmannite phase is prepared by our used method.

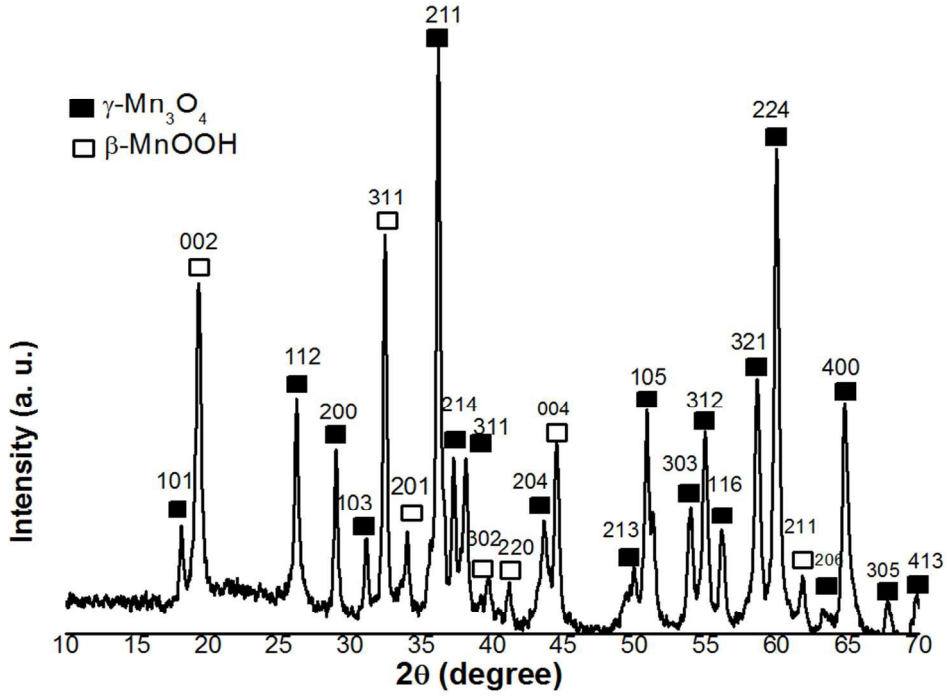

Fig. 1 XRD pattern of the prepared hydrohausmannite.

In order to gain information on the chemical bonds present in the electrodeposited powder, FT-IR studies were carried out in the wavelength range of 400-4000 cm^{-1}. Fig. 2 illustrates FT-IR spectrum of the prepared sample. The bands at 3457 and 1635 cm^{-1} were to the stretching vibration of –OH and the bending vibrations of water molecules. The bands between 800-1400 cm^{-1} (i.e. 1371, 1163, 1048 and 843 cm^{-1}) are typically attributed to the bending vibrations of –OH groups bound with Mn atoms.[24] The peaks in the range of 400-800 cm^{-1} were also indicative of the existence of octahedral MnO6.[25] The two major peaks at 614 and 526 cm^{-1}, were assigned to the coupling between the Mn–O stretching modes of tetrahedral and octahedral sites of Mn_3O_4, respectively.[25,26] The shoulder peak at 565 cm^{-1} and a major

one at 444 cm^{-1} were also assigned to the stretching modes of Mn–O in MnOOH.[27] Based on these results, the IR analysis reconfirmed the formation of mixed Mn_3O_4 and MnOOH phases (i.e. hydrohausmannite), which was in accordance with XRD results (Fig. 1).

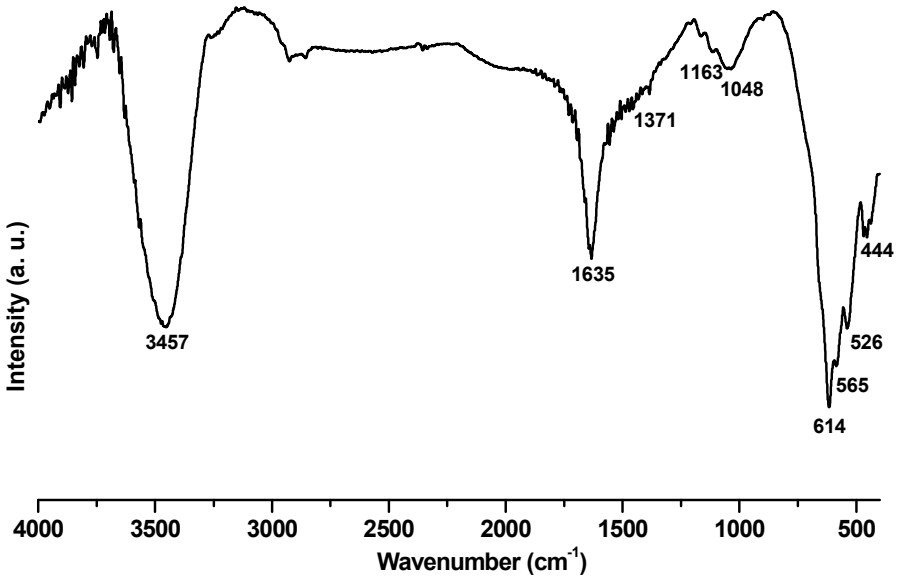

Fig. 2 IR spectrum of the prepared hydrohausmannite

3.2 Morphological characterization

Morphological characteristics of the sample are shown in the SEM images in Fig. 3, which show that the sample is composed of both particle- and plate-like structures. In fact, a major portion of the prepared hydrohausmannite was found to have plate-like structures, while the rest had particle morphology. These observations were in good agreements with those in previous reports,[6-8] which stated that hexagonal plates and particles in hydrohausmannite are generally recognized as *β*-MnOOH and *γ*-Mn_3O_4, respectively.[7] So, based on this fact and the SEM results, it can be restated that the sample is composed of two MnOOH and *γ*-Mn_3O_4 phases which is the characteristic of hydrohausmannite. However, since Da *et al.* have previously reported that γ-Mn_3O_4 and β-MnOOH in hydrohausmannite could not be simply recognized based on morphological conclusions, further examinations were conducted.[8] TEM images in Figs. 3c and d also show large portions of plate-like and less quantities of particles for the prepared sample. However, as seen in Fig. 3d, the plates did not possess complete hexagonal shapes since their

edges were irregular. Eventually it was concluded that the prepared hydrohausmannite possessed both plate- and particle-like morphologies.

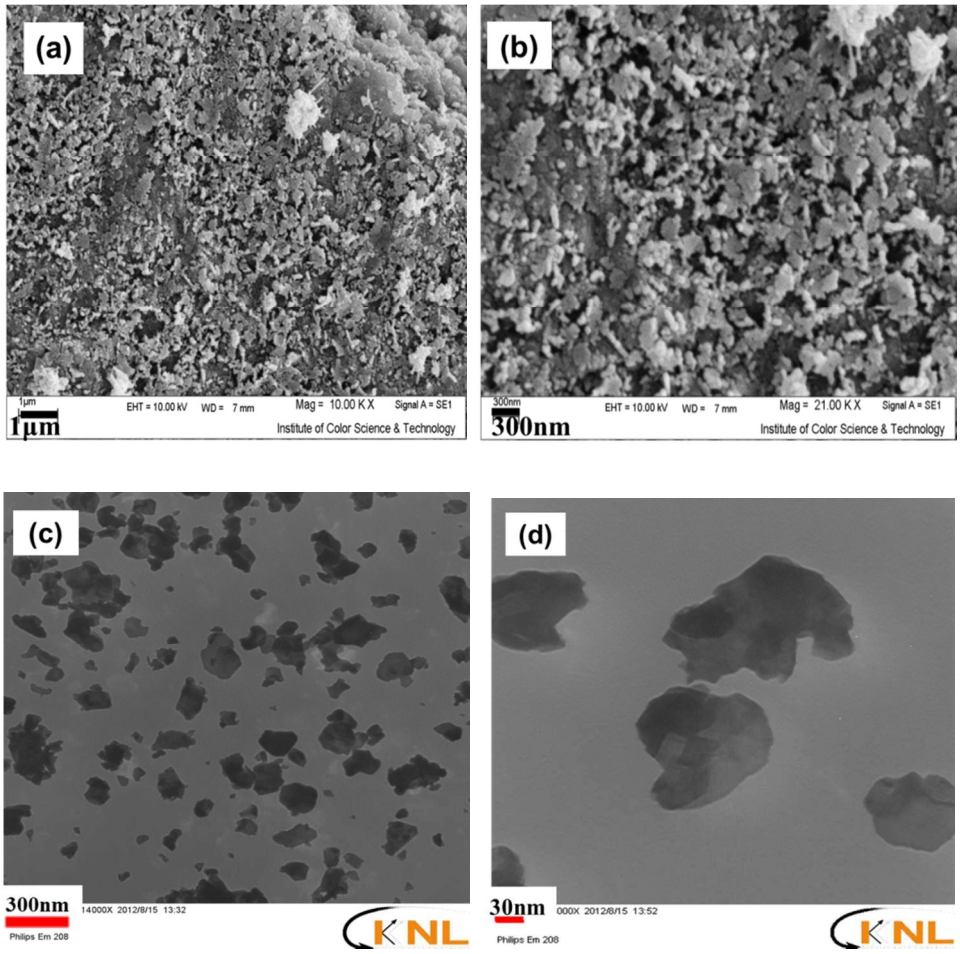

Fig. 3 (a,b) SEM and (c,d) TEM images of the prepared sample.

3.3 Mechanism of formation

Formation of the hydrohausmannite deposit on the cathode surface, from the chloride bath can be probably be explained on the based on a two–step electrochemical–chemical (EC) mechanism[14,15] as shown in Fig. 4, which includes:

- The Electrochemical step:

$O_2 + 2H_2O + 4e^- \rightarrow 4OH^-$ $E^o = +0.26$ V vs. Ag/AgCl (1-1)

$2H_2O + 2e^- \rightarrow H_2 + 2OH^-$ $E^o = -1.08$ V vs. Ag/AgCl (1-2)

where the pH of the solution increases near the steel electrode surface, and by increase in the OH^- concentration, the product deposits on the cathode electrode.

- The Chemical step:

$Mn^{2+}(aq) + 2OH^-(aq) + 1/4O_2 \rightarrow MnOOH + 1/2H_2O$ (2)

$3Mn^{2+}(aq) + 6OH^-(aq) + 1/2O_2 \rightarrow Mn_3O_4 + 3H_2O$ (3)

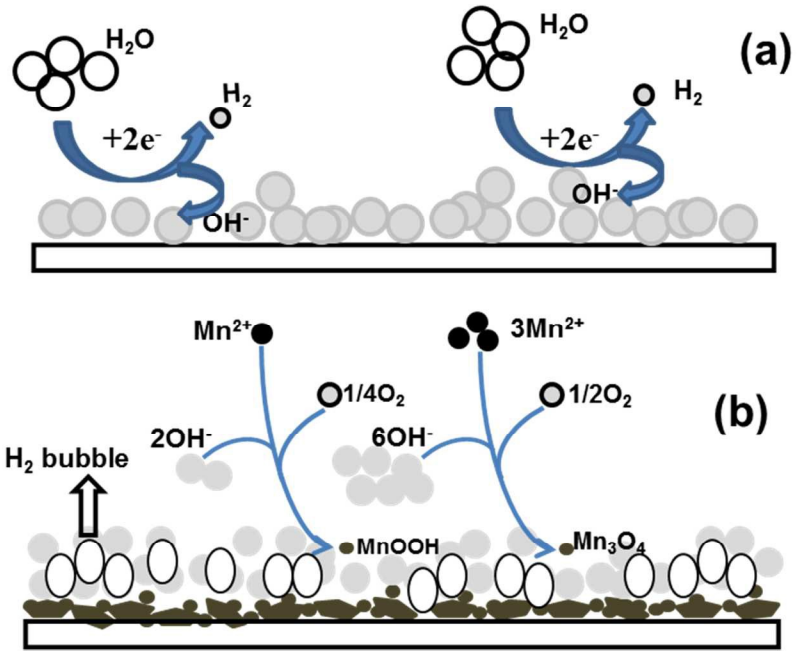

Fig. 4 Schematic view of the proposed mechanism for hydrohausmannite formation *via* the cathodic electrodeposition; (a) electrochemical and (b) chemical steps.

A schematic illustration of these electrochemical and chemical steps is shown in Fig. 4. Considering the value of the observed potential (-1.07V *vs.* Ag/AgCl) during the deposition process, as suggested in the proposed mechanism, the reduction of water (Eq. (1-2)) has a major role in the electrogeneration of base at the applied conditions. In fact, the electrochemical step precedes reactions (1-2) during the deposition process as schematically shown in Fig. 4a. Furthermore, the flow of gas bubbles was observed on the

cathode surface throughout the deposition step, which further confirmed the electrogeneration of OH^- ions due to the electrolysis of water. H_2 bubbles can also affect the surface morphology of the deposit and also act as a dynamic template for the formation and the growth of deposit.[28] In the chemical step, Mn^{2+} cations can react with the OH^- ions produced on electrochemical step in two different ways, which can result in the formation of MnOOH (Eq. 2) and Mn_3O_4 (Eq. 3) deposits, as schematically shown in Fig. 4b. For the formation of hydrohausmannite on the cathode surface, the chemical step should be proceeded via both mentioned ways (Eqs. 1 and 2). Notably, the composition of the deposited sample (i.e. Mn_3O_4 to MnOOH ratio) is directly related to the rates of 2 and 3 reactions. And morphology of the deposit is also dedicated by these reactions (i.e. rates of formation and growth steps).

3.4 Electrochemical evaluation

In order to explore the electrochemical properties of the working electrode fabricated using the deposited hydrohausmannite, cyclic voltammetry (CV) at various scan rates within an electrochemical window from -0.2 V to 0.8 V, was carried out and the corresponding CV curves are shown in Fig. 5a. Obviously, the CV curves of hydrohausmannite show some derivation from a rectangular shape even at low san rate of 5 mV/s, indicating the pseudocapacitance behavior of the fabricated electrode. Notably, the mechanism of supercapacitive performance of hydrohausmannite has not been reported so far, and there is only one report on the electrochemical performance of hydrohausmannite,[9] where it has been reported that hexagonal hydrohausmannite plates prepared via a hydrothermal method are capable of delivering a high specific capacitance (222.4 F g^{-1} at 0.1 A g^{-1}) and good rate capability (66.7 F g^{-1} at 6 A g^{-1}), which has been attributed to their hexagonal structure. Also, it has been observed that the performance becomes even better after cycling, due to the formation of birnessite. However, the charge-discharge process of

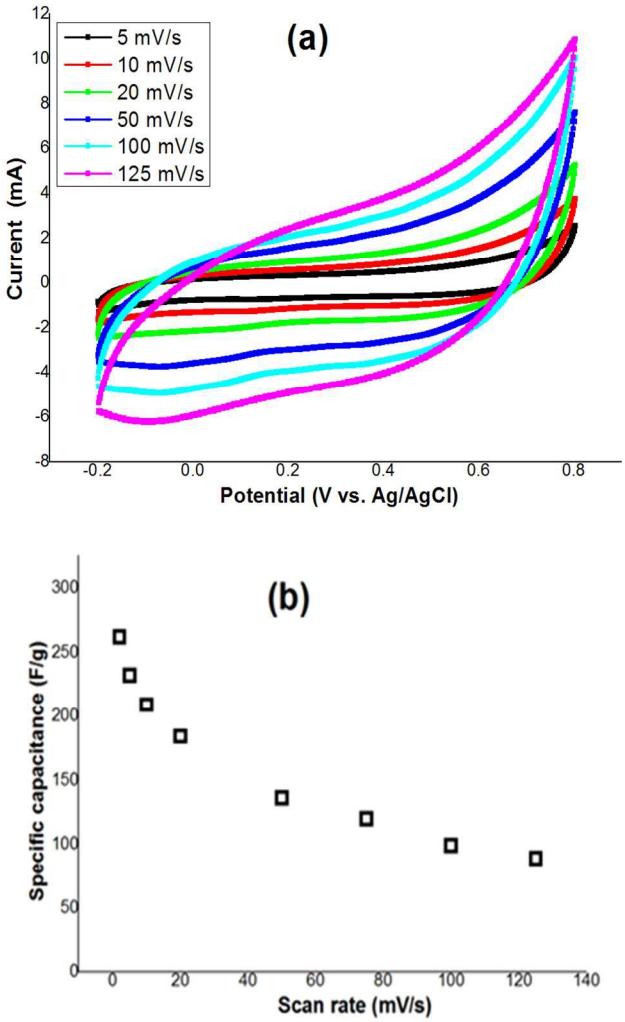

Fig. 5 (a) Cyclic voltammograms of the prepared electrode at various scan rates, and (b) the observed specific capacitance versus scan rates of 2 to 100 mV s^{-1}.

hydrohausmannite has been not described yet. The pseudocapacitance behavior of hydrohausmannite in presence of Na_2SO_4 can be explained based on the following mechanism:

For Mn_3O_4 species:[28,29]

$$Mn_3O_4 + \delta Na^+ + \delta e^- + H_2O \rightarrow Na_\delta MnO_x.nH_2O \quad (4)$$

$$Na_\delta MnO_x.nH_2O + yH^+ + zNa^+ + (y+Z)e^- \leftrightarrow Na_{\delta+z}MnO_x.nH_2O \quad (5)$$

For MnOOH species:[30,31]

$MnOOH \leftrightarrow MnO_2 + H^+ + e^-$ (6)

$MnO_2 + Na^+ + e^- \leftrightarrow MnOOH$ (7)

The nano-particle/plate morphology of the prepared hydrohausmannite can greatly reduce the diffusion length throughout the active materials, where Na^+ must transfer during the charge/discharge process. These characteristics can also provide the electrochemical better utilization of Mn_3O_4 and MnOOH. The specific capacitance values can be calculated by integrating the area of the CV curves as follows:

$$C = \frac{1}{m\vartheta(\Delta V)} \int_{V_a}^{V_c} I(V)\mathrm{d}V \quad (8)$$

where C is the specific capacitance (F g^{-1}), ΔV is the potential range (1 V), *m* is the mass of hydrohausmannite (g), *v* is the scan rate (V s^{-1}), and I(V) is the current response. Using Eq. (8), specific capacitances of 232, 209, 184, 133, 99 and 89 F g^{-1} were calculated at the scan rates of 5, 10, 20, 50, 100 and 125 mV s^{-1}, respectively (Fig. 5b). These values confirmed the excellent supercapacitive performance of the prepared hydrohausmannite. Furthermore, these values are comparable with the reported ones for the Mn_3O_4, MnO_x or MnOOH nanomaterials. For example, 235.4 F g^{-1} at the scan rate of 10 mV s^{-1} for Mn_3O_4 nanospheres [15], 234 F g^{-1} at the scan rate of 5 mV s^{-1} for Mn_3O_4 nanomaterial [30], 220 F g^{-1} at the scan rate 5 mV s^{-1} for α-MnO_2 nanotubes [32], 237 F g^{-1} at the scan rate of 2 mV s^{-1} for MnO_2 nanowires [33], 338 F g^{-1} at the scan rate of 10 mV s^{-1} for α-MnO_2 nanorods [34], 327 F g^{-1} at the scan rate of 2 mV s^{-1} for multiwalled carbon nanotube/α-MnOOH coaxial nanocable [35], 326 F g^{-1} at the scan rate of 2 mV s^{-1} for the electrodeposited MnO_2 on carbon nanotube array [36], 168 F g^{-1} at the scan rate of 10 mV s^{-1} for urchin-like α-MnO_2 nanostructures [37], 151 F g^{-1} at the scan rate of 20 mV s^{-1} for porous Mn_2O_3 nanocubics [38] and 372 F g^{-1} at the scan rate of 25 mV s^{-1} for graphen-MnO_2-CNT composite [39]. Comparing the supercapacitive performance of our prepared electrode with these data reported in the literature for various types of manganese oxide confirmed the acceptable electrochemical performance of hydrohausmannite and makes it as a potential candidate for supercapacitor electrode material.

The dependence of the calculated capacitance on the scan rate of CV from 5 to 125 mV s^{-1} is shown in Fig. 5b. Based on the proposed mechanism, it can be said that increasing the scan rate has a direct impact on the diffusion of Na^+ into the hydrohausmannite matrix. At low scan rates (e.g. 5 mV s^{-1}), the reactions of 4 and 6 will have enough time to proceed, and Na^+ can also easily diffuse into almost all available materials of the electrode, leading to a complete insertion reaction in Eqs. 5 and 7, and hence a better capacitive performance, where a high value of specific capacitance (232 F g^{-1}) is observed. However, increasing the scan rate has a direct impact on the progress of reactions and the diffusion of Na^+ into the hydrohausmannite and also the observed capacitance as seen in Fig. 5b. At a high scan rate (125 mV s^{-1}), reactions 4 and 6 will not have enough time to develop, and further Na^+ will only approach the outer surface of the electrode. Hence due to the great reduction of effective interactions among the ions and the electrode, the capacity loss becomes relatively high (Fig. 5b). However, the prepared hydrohausmannite revealed to be capable of exhibiting a good electrochemical performance i.e. 89 F g^{-1} at the high scan rate of 125 mV s^{-1}.

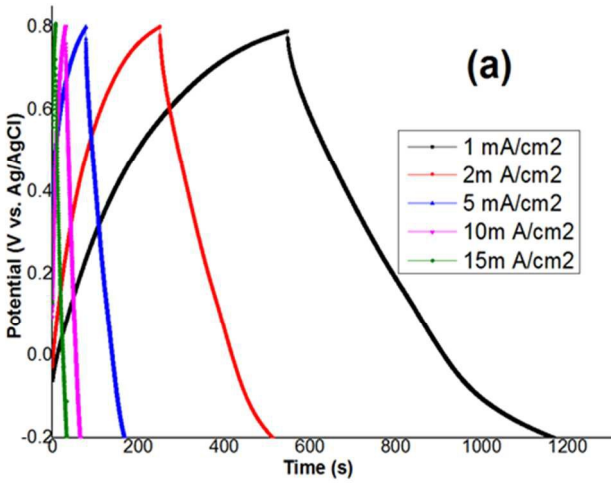

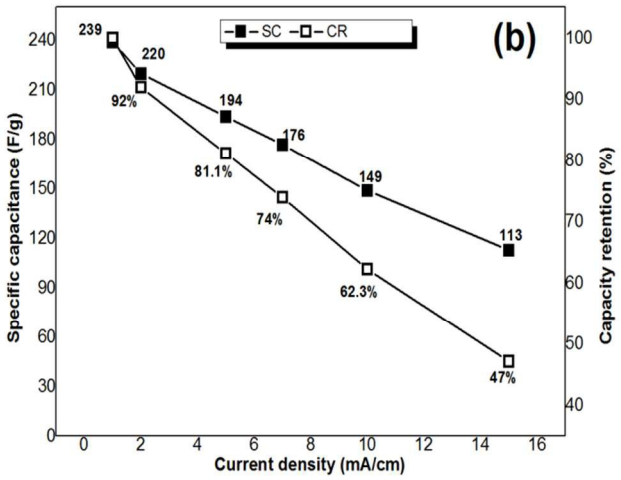

Fig. 6 (a) Chare-discharge profiles of the prepared electrode from hydrohausmannite at various current densities and (b) Calculated specific capacities and capacity retentions values at the current densities of 1, 2, 5, 7, 10 and 15 mA cm^{-2}.

The galvanostatic technology is a reliable experiment to evaluate the specific capacitance values. Fig. 6 shows the charge–discharge curves of Mn_3O_4 nanorods at the current densities of 1, 2, 3, 5, 10 and 15 A g^{-1}. The specific capacitance (SC) of the Mn_3O_4 electrode can be calculated according to the following equation:

$$C = \frac{I \times \Delta t}{m \times \Delta V} \qquad (9)$$

where I is the applied constant current (A), *m* is the mass of $MnMn_2O_4$, ΔV is the potential window during cycling and Δt is the time of a cycle (s). Using Eq (9), and based on the calculations, the nanoplates were expected to be capable of delivering capacitances as high as 239, 220, 194, 176, 149 and 113 F g^{-1} at the applied current densities of 1, 2, 5, 7, 10 and 15 mA cm^{-2}, respectively. The capacity retention versus the applied current density was also calculated and is shown in Fig. 6b. As can be seen in Fig. 6b, the prepared electrode showed capacity retentions of 92%, 81%, 74%, 62% and 47% at the applied current densities of 2, 5, 7, 10 and 15 mA cm^{-2}, respectively, as compared to the low applied current density of 1 mA cm^{-2}. These values confirmed the good electrochemical performance of the prepared electrode. Also the capacitance values, calculated from the charge-discharge curves were in agreements with the calculated ones from the CVs (Fig. 5b).

To investigate the cyclability, the working electrode was cycled (1000 cycling) at the different current densities, and the results for the first 5 cycles of each applied current density are shown in Fig. 7(a1-d1). A little variation from linear shape of potential during both charging and discharging processes was observed, indicating the pseudocapacitance performance of the prepared electrode. The specific capacitance of each cycle at the applied current density was calculated using Eq (8), and is shown in Fig. 7(a2-d2). Also based on the obtained capacitance values, the capacity retention of the fabricated electrode on cycling was evaluated and depicted against cycle number in Fig. 7(a2-d2). The results showed that hydrohausmannite reveals highly stable capacitance behaviours during cycling where high capacity retentions of 91.1%, 89.3%, 84.2%, 80.5% and 74.5% where observed after 1000 charge–discharge cycles at the current densities of 1, 2, 5, 10 and 15 mA cm^{-2}, respectively (Figs. 7(a2-e2)). These results confirmed the excellent supercapacitive performance of the prepared hydrohausmannite.

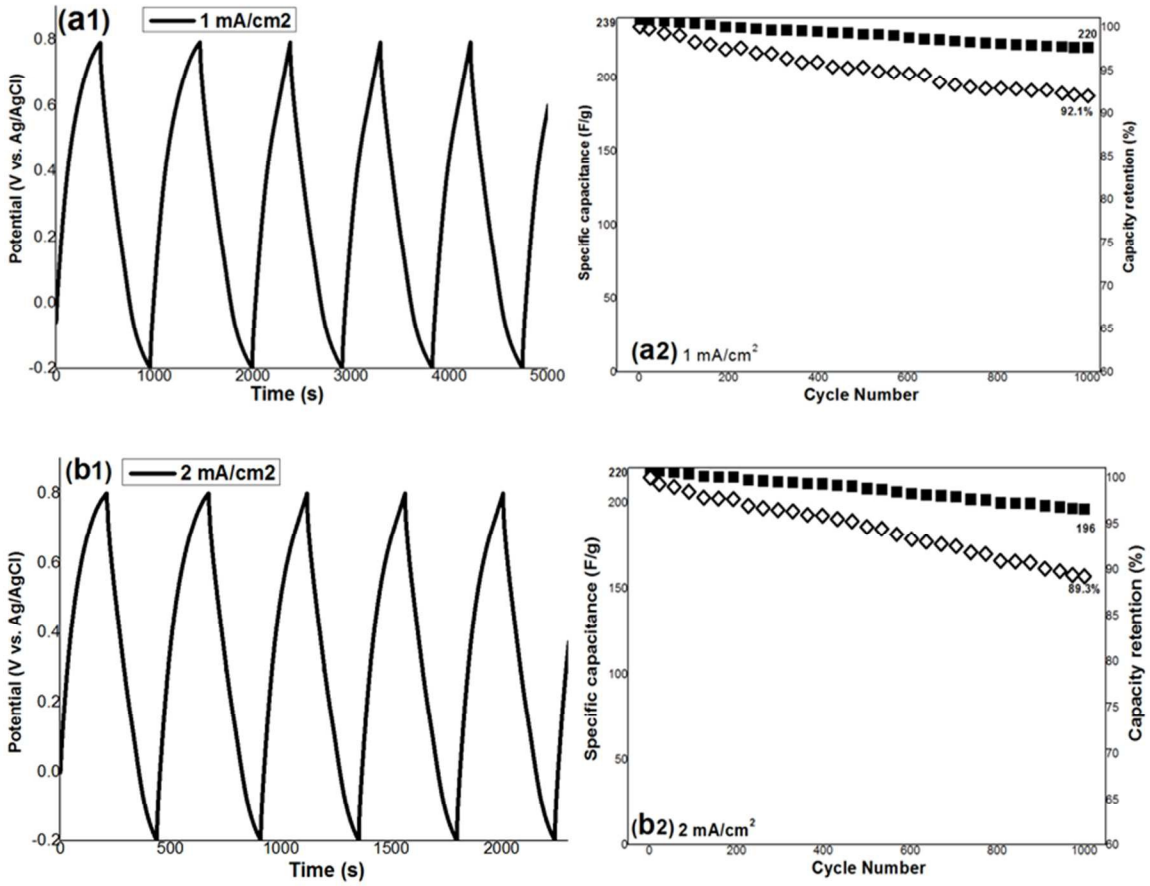

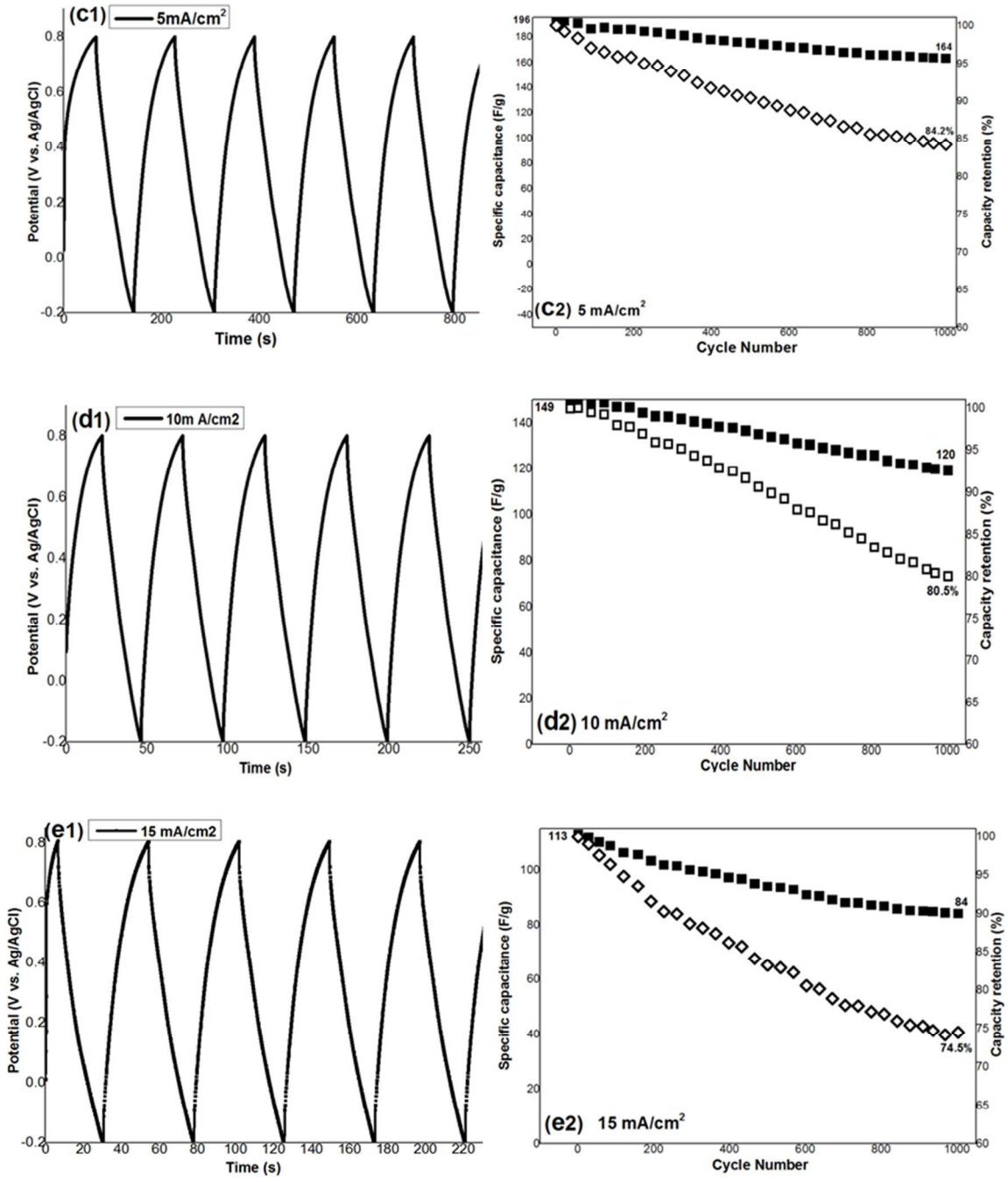

Fig. 7 charge-discharge (first 5 cycles) profiles of the prepared electrode at different applied current densities of (a1) 1, (b1) 2, (c1) 5, (d1) 10 and (e1) 15 mA cm^{-2}, and (a2-e2) the observed specific capacities and capacity retentions after 1000 cycles.

4 Conclusion

For the first time, hydrohausmannite was prepared through a galvanostatic cathodic electrodeposition procedure, from aqueous $MnCl_2$ solution. The electrochemical measurements by cyclic voltammetry and charge-discharge techniques revealed the produced nanostructures to have excellent pseudocapacitive behaviors of high specific capacitances and stable cycle life at various applied current densities. The results marked hydrohausmannite as a potential candidate for use as the electrode material in supercapacitors, and also introduce cathodic electrodeposition as a method that can be used for the preparation of hydrohausmannite under simple operating conditions.

References

1 P. Simon and Y. Gogotsi, *Nature Mater.*, 2008, **7**, 845-854.

2 C. Liu, Z. Yu, D. Neff, A. Zhamu, and B. Z. Jang, *Nano Lett.*, 2010, **10**, 4863-4868.

3 L. Wang, Y. Li, Z. Han, L. Chen, B. Qian, X. Jiang, J. Pinto and G. Yang, *J. Mater. Chem. A*, 2013, **1**, 8385–8397

4 D. -Y. Youn, H. L. Tuller, T. -S. Hyun, D. -K. Choi and I. -D. Kim, *J. Electrochem. Soc.*, 2011, **158**, A970-A975.

5 Z. Liu, Y. Xing, S. Fang , X. Qu, D. Wu, A. Zhang and B. Xu, RSC Adv., Accepted

6 W. Feitknecht and W. Marti, *Helv. Chim. Acta*, 1945, **28**, 129-147.

7 O. Bricker, *Am. Mineral.*, 1965, **50**, 1296-1354.

8 D. Yan, Y. Li, Y. Liu, R. Zhuo, Z. Wu and J. Wang, *Appl. Mechan. Mater.*, 2014, **513**, 277-280.

9 D. Yan, Y. Li , Y. Liu, R. Zhuo, Z. Wu, B. Geng, J. Wang, P. Ren, P. Yan and Z. Geng, *Mater. Lett.*, 2014, **117**, 62–65.

10 B. G. Choi, Y. S. Huh, W. H. Hong, H. J. Kim and H. S. Park, *Nanoscale*, 2012, **4**, 5394-5400.

11 A. Biswal, B. C. Tripathy, K. Sanjay, T. Subbaiahbcd and M. Minakshi, *RSC Adv.*, 2015, **5**, 58255-58283.

12 G. -R. Li, H. Xu, X. -F. Lu, J. -X. Feng, Y. -X. Tong and C. -Y. Su, *Nanoscale*, 2013, **5**, 4056-4069.

13 P. Si, P. Chen and D. -H. Kim, *J. Mater. Chem. B*, 2013, **1**, 2696-2700.

14 T. Yousefi, A. Nozad Golikand, M. H. Mashhadizadeh and M. Aghazadeh, *J. Taiwan Inst. Chem. Eng.*, 2012, **43**, 614-618.

15 T. Yousefi, A. Nozad Golikand, M. H. Mashhadizadeh, and M. Aghazadeh, *Curr. Appl. Phys.*, 2012, **12**, 544-549.

16 Z. Gui, E. Gillette, J. Duay, J. Hu, N. Kim and S. B. Lee, *Phys. Chem. Chem. Phys.*, 2015, **17**, 15173-15180.

17 A. Biswal, B. C. Tripathy, D. Li and M. Minakshi, *Dalton Trans.*, 2015, **44**, 16446-16457.

18 Z. Sun, S. Firdoz, E. Ying-Xuan Yap, L. Li and X. Lu, *Nanoscale*, 2013, **5**, 4379-4387.

19 Y. Qiu, P. Xu, B. Guo, Z. Cheng, H. Fan, M. Yang, X. Yang and J. Li, *RSC Adv.*, 2014, **4**, 64187-6419.

20 J. Duay, E. Gillette, J. Hu and S. B. Lee, *Phys. Chem. Chem. Phys.*, 2013, **15**, 7976-7993.

21 P. Yang, Y. Li, Z. Lin, Y. Ding, S. Yue, C. P. Wong, X. Cai, S. Tan and W. Mai, *J. Mater. Chem. A*, 2014, **2**, 595-599.

22 J. Shabani, A. Ehsani, A. Nikkar, P. Norouzi, M. R. Ganjali and M. wojdyla, New J. Chem., 2015, Accepted Manuscript, DOI: 10.1039/C5NJ01954K.

23 J. Shabani, P. Norouzi, M. R. Ganjali, M. Wojdyla, K. Fic and E. Frackowiak, *RSC Adv.*, 2015, Accepted Manuscript, DOI: 10.1039/C5RA11962F.

24 Zhenxin Liu, Yu Xing, Shaoming Fang, Xiongwei Qu, Depeng Wu, Aiqin Zhang and Bei Xu, RSC Adv., 2015, **5**, 54867-54872.

25 W. Zhang, Z. Yang, Y. Liu, S. Tang, X. Han and M. Chen, *J. Cryst. Growth*, 2004, **263**, 394-399.

26 Y. Li and and X. M. Li, *RSC Adv.*, 2013, **3**, 2398-2403.

27 Z. Li, H. Bao, X. Miao and X. Chen, *J. Colloid and Interface Sci.*, 2011, **357**, 286–291.

28 F. Khosrow-pour, M. Aghazadeh and B. Arhami, J. Electrochem. Soc., 2013, **160**, D150-D155.

29 Y. Dai, K. Wang and J. Xie, *Appl. Phys. Lett.,* 2007, **90**, 104102–104103.

30 D. P. Dubal, D. S. Dhawale, R. R. Salunkhe and C. D. Lokhande, *J. Electroanal. Chem.*, 2010, **647**, 60–65.

31 S. Devaraj and N. Munichandraiah, *J. Phys. Chem. C*, 2008, **112**, 4406-4417.

32 W. Xiao, H. Xia, J.Y.H. Fuh and L. Lu, *J. Power Sour.*, 2009, **193**, 935-938.

33 T. Yousefi, A.N. Golikand, M.H. Mashhadizadeh and M. Aghazadeh, *Curr. Appl. Phys.*, 2012, **12**, 193-198.

34 T. Yousefi, A.N. Golikand, M.H. Mashhadizadeh and M. Aghazadeh, *J. Solid State Chem.*, 2012, **190**, 202-207.

35 H. Fang, S. Zhang, X. Wu, W. Liu, B. Wen, Z. Du and T. Jiang, *J. Power Sour.*, 2013, **235**, 95-104.

36 P. Lv, P. Zhang, Y. Feng, Y. Li and W. Feng, *Electrochim. Acta*, 2012, **78**, 515-523.

37 S. Zhao, T. Liu, D. Shi, Y. Zhang, W. Zeng, T. Li, B. Miao, *Appl. Surf. Sci.*, 2015, **351**, 862–868.

38 W. Li, J. Shao, Q. Liu, X. Liu, X. Zhou and J. Hu, *Electrochim. Acta*, 2015, **157**, 108-114.

39 Y. Cheng, S. Lu, H. Zhang, C.V. Varanasi and J. Liu, *Nano Lett.*, 2012, **12**, 4206-4211.